J. Nonlinear Funct. Anal. 2026 (2026) 14 https://doi.org/10.23952/jnfa.2026.14

MATHRES Journal of Nonlinear Functional Analysis
Available online at http://jnfa.mathres.org

DELAY AND NEUTRAL-TERM ORDER-REGULATED STABILITY IN FOUR-NEURON FRACTIONAL-ORDER RECURRENT NEURAL NETWORKS

HONGFEI XU[1], CHENGDAI HUANG[2], HENG LIU[3], LIPING ZHOU[1,*]

[1]College of Science, Hunan University of Science and Engineering, Yongzhou 425199, China
[2]School of Mathematics and Statistic, Xinyang Normal University, Xinyang 464000, China
[3]School of Mathematics and Physics, Guangxi Minzu University, Nanning 530006, China

Abstract. Fractional-order neutral-type recurrent neural networks (FONTRNNs) hold promise for dynamic modeling, yet fixed neutral term order in existing studies restricts regulation flexibility. This paper proposes a four-neuron FONTRNN with independently tunable neutral term order. By decoupling the characteristic equation into trigonometric-variable linear systems, we derive explicit delay-dependent stability criteria and Hopf bifurcation points via Cramer's rule. Notably, an extended bifurcation framework is developed by treating the neutral term order as the bifurcation parameter, with critical values solved through implicit function curve intersection. Numerical simulations verify that reducing the derivative order consistently stabilizes the system, while adjusting the neutral term order enhances or weakens stability depending on parameter configurations.

Keywords. Fractional-order neural network; Hopf Bifurcation; Implicit function method; Neutral term fractional order; Stability.

1. INTRODUCTION

Fractional calculus, whose conceptual roots can be traced back to Leibniz's correspondence in 1695, has steadily emerged as a powerful mathematical framework for capturing memory and hereditary properties in complex systems. Notably, the non-local and history-dependent nature of fractional-order models aligns perfectly with the time-varying, memory-endowed dynamics of biological and artificial neural networks. This congruence thereby sets them apart from their integer-order counterparts, which enables their unique capacity to encapsulate nuanced temporal dependencies and frequency adaptation characteristics [1,2]. This capability facilitates its applications in diverse fields, including medical science [3,4], mathematical biology [5,6], circuit design [7], and computational intelligence [8,9].

*Corresponding author.
E-mail address: lpzhuse@163.com (L. ZHOU).
Received December 4, 2025; Accepted March 2, 2026.

At a neurobiological level, experimental work has reinforced the relevance of this mathematical tool, revealing that neuronal responses naturally conform to fractional differentiation principles [10]. Importantly, such dynamics empower neurons with fundamental processing abilities such as temporal memory encoding and adaptive frequency modulation. These findings provide a solid foundation for integrating fractional-order operators into neural network modeling, leading to more faithful representations of neural dynamics [11]. Beyond representational accuracy, the resulting fractional-order framework enhances not only the expressive power of networks but also their resilience to input delays and external disturbances [12]. These strengths have subsequently spurred considerable theoretical research into the dynamics of such networks, particularly regarding stability [13, 14], bifurcation mechanisms [15, 16], and synchronization phenomena [17, 18].

However, a central challenge in modelling realistic neural networks stems from the ubiquitous presence of time delays caused by finite signal transmission speeds in both biological and electronic systems [19,20]. While conventional delays have received extensive attention, a more subtle and complex scenario arises with neutral-type delays, which incorporate lags directly into the derivative components of the system's states [21]. This structure couples the history of state derivatives with the system's current evolution, yielding a richer and more intricate dynamical landscape, including stability switches and Hopf bifurcations, which is particularly relevant for simulating biological neural processes and cellular dynamics [22]. Although the inclusion of neutral delays enhances bioplausibility, it comes at a price: substantial complications in stability and bifurcation analysis due to the infinite-dimensional nature of the resulting equations and the accompanying transcendental characteristic terms [23, 24].

In recent years, the field of fractional-order delayed neural networks (FODNNs) has witnessed remarkable progress, with researchers formulating refined stability criteria [25], unraveling delay-induced bifurcation mechanisms [26], and devising order-dependent control strategies [27]. This progress has naturally extended into the realm of fractional-order neutral-type neural networks (FONNTNNs), where studies have explored asymptotic stability and synchronization in memristive networks with time delays [28], established enhanced stability criteria via sophisticated Lyapunov methods [29], and uncovered intriguing bifurcation phenomena—though often still within the confines of small-scale neuronal models [21, 30, 31].

Despite these advances, a closer examination reveals several interconnected limitations in current research. First, a fundamental issue lies in the widespread assumption that the neutral term order equals the fractional derivative order—a simplification that fails to capture the distinct memory properties observed in biological neural processes, where mechanisms like synaptic transmission and membrane recovery operate at different timescales [32]. Furthermore, this conceptual limitation is compounded by a notable gap in systematic investigations. Specifically, few studies have treated the neutral term order as an independent bifurcation parameter. While some studies have explored bifurcations induced by the fractional order while overlooking neutral delay effects [27], others have focused exclusively on conventional parameters like time delays as bifurcation triggers [33], leaving the unique role of neutral order in driving oscillatory transitions largely unexamined. Additionally, when employing orders as bifurcation parameters, the characteristic equation of fractional-order neutral systems exhibits enhanced complexity near criticality, posing significant challenges for standard analytical methods [22, 25] to derive explicit stability conditions dependent on the neutral term order.

Recurrent neural networks (RNNs) effectively simulate feedback mechanisms found throughout biological brains. These mechanisms underlie critical neural functions including oscillations, pattern storage, and attentional modulation [34]. Building on this foundation, we propose a fractional-order neutral-type RNN featuring independently tunable neutral and derivative orders. This architectural innovation offers necessary flexibility for more accurately capturing the multi-timescale dynamics of biological neural systems. The main contributions of this work are summarized as follows:

1) We propose a novel four-neuron model with an independently tunable neutral term order, distinct from both the left-hand side and fractional derivative orders. Unlike conventional models [30, 35] constraining these orders to equality, this design offers targeted matching of diverse memory decay characteristics in complex systems, providing extra degrees of freedom while preserving theoretical rigor.
2) We resolve the $e^{4s\tau}$ computational bottleneck in high-dimensional neutral delayed networks, establish the Hopf criterion for high-dimensional systems, and reveal distinct regulatory roles of derivative and neutral orders in bifurcation thresholds.
3) We propose the neutral-term order as a novel bifurcation parameter, developing a dedicated theoretical framework to extend Hopf analysis via implicit function curve intersection for accurate identification of critical values, even in degenerate cases as the neutral order approaches zero.
4) We reveal a novel regulatory mechanism in fractional-order neural networks: unlike the literature-confirmed consistently destabilizing effect of the derivative order [15, 16, 31, 33], the neutral term order exhibits dual regulatory effects capable of enhancing or weakening system stability under varying parameters. This finding establishes a new independent control parameter for precise dynamics manipulation.

This paper is organized as follows. Section 2 integrates mathematical preliminaries and presents the four-neuron fractional-order neutral-type recurrent neural network model. The core theoretical results on bifurcation analysis are established in Section 3. Section 4 offers numerical verification, and the paper is concluded with a summary in Section 5.

2. Preliminaries

In this section, we introduce the Caputo fractional-order derivative and its Laplace transform, and provide a lemma supporting the stability analysis of fractional-order neutral-type neural networks.

Definition 2.1. *[36] Let $\kappa-1<\varrho\leq\kappa\in\mathbb{Z}^+$, and $t\geq a$. The Caputo fractional-order derivative starting at a is given by*

$$ {}_a^C D^{\varrho} f(t)=\frac{1}{\Gamma(\kappa-\varrho)}\int_a^t (t-s)^{\kappa-\varrho-1} f^{(\kappa)}(s)ds, $$

where $\Gamma(\cdot)$ is the Gamma function.

By exploiting the Laplace transformation, we transform the Caputo fractional-order derivative at $a=0$ as follows

$$ \mathscr{L}\{{}_a^C D^{\varrho} f(t);s\}=s^{\varrho}F(s)-\sum_{k=0}^{\kappa-1} s^{\varrho-k-1} f^{(k)}(0), \kappa-1<\varrho\leq\kappa\in\mathbb{Z}^+. \tag{2.1} $$

If $f^{(k)}(0)=0, k=0,1,\ldots,\kappa-1$, then $\mathscr{L}\{{}_a^C D^{\varrho} f(t);s\}=s^{\varrho}F(s)$. For ease of notation, we denote ${}_a^C D^{\varrho}$ by ${}^C D^{\varrho}$.

Lemma 2.2. *[30] Consider the n-dimensional linear neutral delays fractional-order neural network*

$$D^{\varrho}u_i(t) = -a_i u_i(t) + \sum_{j=1}^{n} b_{ij}u_j(t-\tau_{ij}) + \sum_{j=1}^{n} c_{ij}D^{\rho}u_j(t-\tau_{ij}), \tag{2.2}$$

where $0<\varrho<1, 0\le\rho<1$ represent the fractional derivatives order and neutral term fractional order, respectively. The initial values $u_i(t)=\phi_i(t)$ are given for $-max_{i,j}\tau_{ij}=-\tau_{max}\le t\le 0$ and $i,j=1,2,\ldots,n$. $T=(\tau_{ij})_{n\times n}\in(R^{+})_{n\times n}$ is the delay matrix of system (2.2), a_i, b_{ij}, c_{ij} label coefficients, $u_i(t), u_j(t-\tau_{ij})\in\mathbb{R}$ denote state variables, and $\phi_i(t)\in C^0[-\tau_{\max},0]$ represent initial values. Applying (2.1) to (2.2) yields the characteristic matrix

$$\triangle(s)=\begin{bmatrix} \vartheta_{11}(s) & \vartheta_{12}(s) & \cdots & \vartheta_{1n}(s) \\ \vartheta_{21}(s) & \vartheta_{22}(s) & \cdots & \vartheta_{2n}(s) \\ \vdots & \vdots & \ddots & \vdots \\ \vartheta_{n1}(s) & \vartheta_{n2}(s) & \cdots & \vartheta_{nn}(s) \end{bmatrix},$$

where

$$\begin{aligned}
&\vartheta_{11}(s)=s^{\varrho}+a_1-b_{11}e^{-s\tau_{11}}-c_{11}s^{\rho}e^{-s\tau_{11}}, && \vartheta_{12}(s)=-b_{12}e^{-s\tau_{12}}-c_{12}s^{\rho}e^{-s\tau_{12}},\\
&\vartheta_{1n}(s)=-b_{1n}e^{-s\tau_{1n}}-c_{1n}s^{\rho}e^{-s\tau_{1n}}, && \vartheta_{21}(s)=-b_{21}e^{-s\tau_{21}}-c_{21}s^{\rho}e^{-s\tau_{21}},\\
&\vartheta_{22}(s)=s^{\varrho}+a_2-b_{22}e^{-s\tau_{22}}-c_{22}s^{\rho}e^{-s\tau_{22}}, && \vartheta_{2n}(s)=-b_{2n}e^{-s\tau_{2n}}-c_{2n}s^{\rho}e^{-s\tau_{2n}},\\
&\vartheta_{n1}(s)=-b_{n1}e^{-s\tau_{n1}}-c_{n1}s^{\rho}e^{-s\tau_{n1}}, && \vartheta_{n2}(s)=-b_{n2}e^{-s\tau_{n2}}-c_{n2}s^{\rho}e^{-s\tau_{n2}},\\
&\vartheta_{nn}(s)=s^{\varrho}+a_n-b_{nn}e^{-s\tau_{nn}}-c_{nn}s^{\rho}e^{-s\tau_{nn}}.
\end{aligned}$$

If all the roots of the characteristic equation $det(\triangle(s))=0$ have negative real parts, then the origin of system (2.2) is Lyapunov globally asymptotically stable.

Remark 2.3. In contrast to [30, Lemma 1], our model incorporates two distinct orders $\rho\neq\varrho$, which renders the root distribution of the characteristic equation $\triangle(s)=0$ significantly more intricate, thereby making the analysis far more challenging.

We now present the four-neuron fractional-order neutral–type recurrent neural network (FONT RNN) whose neutral term orders are independently tunable. The dynamics of the ith neuron $i=1,\ldots,4$ are described by:

$$\begin{cases}
D^{\varrho}u_1(t) = -u_1(t)+a_1f_2(u_2(t-\tau))+c_1D^{\rho}u_2(t-\tau),\\
D^{\varrho}u_2(t) = -u_2(t)+a_2f_3(u_3(t-\tau))+c_2D^{\rho}u_3(t-\tau),\\
D^{\varrho}u_3(t) = -u_3(t)+a_3f_4(u_4(t-\tau))+c_3D^{\rho}u_4(t-\tau),\\
D^{\varrho}u_4(t) = -u_4(t)+b_1f_1(u_1(t-\tau))+b_2f_2(u_2(t-\tau))+b_3f_3(u_3(t-\tau))\\
\qquad\quad +c_4D^{\rho}u_1(t-\tau)+c_5D^{\rho}u_2(t-\tau)+c_6D^{\rho}u_3(t-\tau),
\end{cases} \tag{2.3}$$

where $u_i(i=1,2,3,4)$ are the state of i-th neuron at time t; $a_j, j=1,2,3$ refer to the internal decay rates; b_j signify the connection weights between neurons; $c_k, k=1,2,\cdots,6$ stand for neutral connection weights; f_i correspond to nonlinear feedback and activation functions respectively;

$0 < \varrho < 1, 0 \le \rho < 1$ represent the orders of the left-hand side and the neutral terms on the right-hand side of the equations, respectively. Henceforth, we assume the following properties for the functions f_i :

(**A**1) $f_i(\cdot) \in C^1(\mathbb{R},\mathbb{R})$, $f_i(0) = 0$ and $u_i f_i(u_i) > 0$ for $u_i \neq 0$.

Remark 2.4. We adopt the Caputo fractional-order derivative, which offers the advantage that its Laplace transform involves only integer-order initial conditions, exhibits a clear physical interpretation, and accurately captures the memory effects and power-law decay characteristics of neurons, making it suitable for modeling realistic neural networks. Regarding the activation functions, we introduce Assumption **A**1. This assumption ensures that the origin is an equilibrium point of the system, the smoothness guarantees the feasibility of linearization, and the sign condition reflects the excitatory-inhibitory mechanism of biological neurons. Moreover, common activation functions such as $\tanh(\cdot)$ satisfy this requirement, facilitating numerical validation. The above settings provide a rigorous foundation for the subsequent stability analysis and the establishment of bifurcation criteria.

Remark 2.5. Setting $c_k = 0$ eliminates the neutral terms and the model reduces to the retarded fractional-order recurrent neural network (FORNN) studied in [37,38]. The present FONTRNN framework thus generalises FORNN and allows one to investigate the effect of distinct neutral orders.

3. Main Results

This section investigates bifurcation phenomena in the proposed FONTRNN model driven by two distinct mechanisms: time delay and neutral-term order.

3.1. Time delay induced bifurcation in FONTRNN.

Under assumption **A**1, the origin is an equilibrium point of FONTRNN (2.3). To analyze the network's stability and bifurcations, we present its linearized equations around the origin

$$\begin{cases} D^{\varrho}u_1(t) = -u_1(t) + d_1u_2(t-\tau) + c_1D^{\rho}u_2(t-\tau), \\ D^{\varrho}u_2(t) = -u_2(t) + d_2u_3(t-\tau) + c_2D^{\rho}u_3(t-\tau), \\ D^{\varrho}u_3(t) = -u_3(t) + d_3u_4(t-\tau) + c_3D^{\rho}u_4(t-\tau), \\ D^{\varrho}u_4(t) = -u_4(t) + m_1u_1(t-\tau) + m_2u_2(t-\tau) + m_3u_3(t-\tau) \\ \qquad\qquad + c_4D^{\rho}u_1(t-\tau) + c_5D^{\rho}u_2(t-\tau) + c_6D^{\rho}u_3(t-\tau), \end{cases} \tag{3.1}$$

where $d_j = a_jf_j'(0), m_j = b_jf_j'(0), j = 1,2,3$.

By Lemma 2.2, we derive the characteristic equation

$$\sum_{k=0}^{4} \mathscr{P}_k(s)\mathrm{e}^{ks\tau} = 0, \tag{3.2}$$

with

$$\begin{aligned} \mathscr{P}_0(s) &= -(c_1s^{\rho}+d_1)(c_2s^{\rho}+d_2)(c_3s^{\rho}+d_3)(c_4s^{\rho}+m_1), \\ \mathscr{P}_1(s) &= -(s^{\varrho}+1)(c_2s^{\rho}+d_2)(c_3s^{\rho}+d_3)(c_5s^{\rho}+m_2), \\ \mathscr{P}_2(s) &= -(s^{\varrho}+1)^2(c_3s^{\rho}+d_3)(c_6s^{\rho}+m_3), \\ \mathscr{P}_3(s) &= 0, \mathscr{P}_4(s) = (s^{\varrho}+1)^4. \end{aligned}$$

Setting $\tau = 0$ in (3.2) eliminates all transcendental terms, and the equation reduces to the algebraic polynomial

$$\sum_{q,p\geq 0, q+p\leq 4} A_{qp} s^{q\rho+p\varrho} = 0, \tag{3.3}$$

where

$$\begin{aligned}
A_{00} =& 1 - d_1d_2d_3m_1 - d_2d_3m_2 - d_3m_3,\\
A_{01} =& - c_1d_2d_3m_1 - c_2d_1d_3m_1 - c_3d_1d_2m_1 - c_4d_1d_2d_3\\
& - c_2d_3m_2 - c_3d_2m_2 - c_5d_2d_3 - c_3m_3 - c_6d_3,\\
A_{02} =& - c_1c_2d_3m_1 - c_1c_3d_2m_1 - c_1c_4d_2d_3 - c_2c_3d_1m_1 - c_2c_4d_1d_3\\
& - c_3c_4d_1d_2 - c_2c_3m_2 - c_2c_5d_3 - c_3c_5d_2 - c_3c_6,\\
A_{03} =& - c_1c_2c_3m_1 - c_1c_2c_4d_3 - c_1c_3c_4d_2 - c_2c_3c_4d_1 - c_2c_3c_5,\\
A_{04} =& - c_1c_2c_3c_4,\\
A_{10} =& 4 - d_2d_3m_2 - 2d_3m_3,\\
A_{11} =& - c_2d_3m_2 - c_3d_2m_2 - c_5d_2d_3 - 2c_3m_3 - 2c_6d_3,\\
A_{12} =& - c_2c_3m_2 - c_2c_5d_3 - c_3c_5d_2 - 2c_3c_6,\\
A_{13} =& - c_3c_6, A_{20} = 6 - d_3m_3, A_{21} = -c_3m_3 - c_6d_3,\\
A_{22} =& - c_3c_6, A_{30} = 4, A_{31} = 0, A_{40} = 1.
\end{aligned}$$

Lemma 2.2 guarantees that the origin of (2.3) is asymptotically stable provided all roots of (3.3) have negative real parts. For $\tau > 0$, we aim to determine the critical delay value for model (2.3) beyond which the system loses stability. To this end, we multiply equation (3.2) by $e^{-s\tau}$, $e^{-2s\tau}$, and $e^{-3s\tau}$, respectively on both sides, yielding three derived equations with lower-order transcendental terms

$$\begin{cases}
\mathscr{P}_0(s)e^{-s\tau} + \mathscr{P}_1(s) + \mathscr{P}_2(s)e^{s\tau} + \mathscr{P}_4(s)e^{3s\tau} = 0,\\
\mathscr{P}_0(s)e^{-2s\tau} + \mathscr{P}_1(s)e^{-s\tau} + \mathscr{P}_2(s) + \mathscr{P}_4(s)e^{2s\tau} = 0,\\
\mathscr{P}_0(s)e^{-3s\tau} + \mathscr{P}_1(s)e^{-2s\tau} + \mathscr{P}_2(s)e^{-s\tau} + \mathscr{P}_4(s)e^{s\tau} = 0.
\end{cases} \tag{3.4}$$

Suppose that a purely imaginary root $s = i\xi$ satisfies (3.4), for which we express $\mathscr{P}_J(i\xi) = \mathscr{P}_J^R(\xi) + i\mathscr{P}_J^I(\xi)$ for $J = 0, 1, 2, 4$ and separate the real and imaginary parts, yielding a linear trigonometric system

$$\begin{cases}
l_{11}\cos\xi\tau + l_{12}\sin\xi\tau + l_{13}\cos 2\xi\tau + l_{14}\sin 2\xi\tau + l_{15}\cos 3\xi\tau + l_{16}\sin 3\xi\tau = -\mathscr{P}_1^R,\\
l_{21}\cos\xi\tau + l_{22}\sin\xi\tau + l_{23}\cos 2\xi\tau + l_{24}\sin 2\xi\tau + l_{25}\cos 3\xi\tau + l_{26}\sin 3\xi\tau = -\mathscr{P}_1^I,\\
l_{31}\cos\xi\tau + l_{32}\sin\xi\tau + l_{33}\cos 2\xi\tau + l_{34}\sin 2\xi\tau + l_{35}\cos 3\xi\tau + l_{36}\sin 3\xi\tau = -\mathscr{P}_2^R,\\
l_{41}\cos\xi\tau + l_{42}\sin\xi\tau + l_{43}\cos 2\xi\tau + l_{44}\sin 2\xi\tau + l_{45}\cos 3\xi\tau + l_{46}\sin 3\xi\tau = -\mathscr{P}_2^I,\\
l_{51}\cos\xi\tau + l_{52}\sin\xi\tau + l_{53}\cos 2\xi\tau + l_{54}\sin 2\xi\tau + l_{55}\cos 3\xi\tau + l_{56}\sin 3\xi\tau = 0,\\
l_{61}\cos\xi\tau + l_{62}\sin\xi\tau + l_{63}\cos 2\xi\tau + l_{64}\sin 2\xi\tau + l_{65}\cos 3\xi\tau + l_{66}\sin 3\xi\tau = 0,
\end{cases} \tag{3.5}$$

where

$$
\begin{aligned}
&l_{11}=\mathscr{P}_0^R+\mathscr{P}_2^R, l_{12}=\mathscr{P}_0^I-\mathscr{P}_2^I, l_{13}=0, l_{14}=0, l_{15}=\mathscr{P}_4^R, l_{16}=-\mathscr{P}_4^I,\\
&l_{21}=\mathscr{P}_0^I+\mathscr{P}_2^I, l_{22}=-\mathscr{P}_0^R+\mathscr{P}_2^R, l_{23}=0, l_{24}=0, l_{25}=\mathscr{P}_4^I, l_{26}=\mathscr{P}_4^R,\\
&l_{31}=\mathscr{P}_1^R, l_{32}=\mathscr{P}_1^I, l_{33}=\mathscr{P}_0^R+\mathscr{P}_4^R, l_{34}=\mathscr{P}_0^I-\mathscr{P}_4^I, l_{35}=0, l_{36}=0,\\
&l_{41}=\mathscr{P}_1^I, l_{42}=-\mathscr{P}_1^R, l_{43}=\mathscr{P}_0^I+\mathscr{P}_4^I, l_{44}=-\mathscr{P}_0^R+\mathscr{P}_4^R, l_{45}=0, l_{46}=0,\\
&l_{51}=\mathscr{P}_2^R+\mathscr{P}_4^R, l_{52}=\mathscr{P}_2^I-\mathscr{P}_4^I, l_{53}=\mathscr{P}_1^R, l_{54}=\mathscr{P}_1^I, l_{55}=\mathscr{P}_0^R, l_{56}=\mathscr{P}_0^I,\\
&l_{61}=\mathscr{P}_2^I+\mathscr{P}_4^I, l_{62}=-\mathscr{P}_2^R+\mathscr{P}_4^R, l_{63}=\mathscr{P}_1^I, l_{64}=-\mathscr{P}_1^R, l_{65}=\mathscr{P}_0^I, l_{66}=-\mathscr{P}_0^R,
\end{aligned}
$$

and

$$
\begin{aligned}
\mathscr{P}_0^R=&-c_1c_2c_3c_4\cos 2\pi\rho\cdot\xi^{4\rho}-(c_1c_2c_3m_1+c_1c_2c_4d_3+c_1c_3c_4d_2+c_2c_3c_4d_1)\cos\frac{3\pi\rho}{2}\cdot\xi^{3\rho}\\
&-(c_1c_2d_3m_1+c_1c_3d_2m_1+c_1c_4d_2d_3+c_2c_3d_1m_1+c_2c_4d_1d_3+c_3c_4d_1d_2)\cos\pi\rho\cdot\xi^{2\rho}\\
&-(c_1d_2d_3m_1+c_2d_1d_3m_1+c_3d_1d_2m_1+c_4d_1d_2d_3)\cos\frac{\pi\rho}{2}\cdot\xi^{\rho}-d_1d_2d_3m_1,\\
\mathscr{P}_0^I=&-c_1c_2c_3c_4\sin 2\pi\rho\cdot\xi^{4\rho}-(c_1c_2c_3m_1+c_1c_2c_4d_3+c_1c_3c_4d_2+c_2c_3c_4d_1)\sin\frac{3\pi\rho}{2}\cdot\xi^{3\rho}\\
&-(c_1c_2d_3m_1+c_1c_3d_2m_1+c_1c_4d_2d_3+c_2c_3d_1m_1+c_2c_4d_1d_3+c_3c_4d_1d_2)\sin\pi\rho\cdot\xi^{2\rho}\\
&-(c_1d_2d_3m_1+c_2d_1d_3m_1+c_3d_1d_2m_1+c_4d_1d_2d_3)\sin\frac{\pi\rho}{2}\cdot\xi^{\rho},\\
\mathscr{P}_1^R=&-c_2c_3c_5\cos\frac{\pi}{2}(\varrho+3\rho)\cdot\xi^{\varrho+3\rho}-(c_2c_3m_2+c_3c_5d_2+c_2c_5d_3)\cos\frac{\pi}{2}(\varrho+2\rho)\cdot\xi^{\varrho+2\rho}\\
&-c_2c_3c_5\cos\frac{3\pi\rho}{2}\cdot\xi^{3\rho}-(c_3d_2m_2+c_2d_3m_2+c_5d_2d_3)\cos\frac{\pi}{2}(\varrho+\rho)\cdot\xi^{\varrho+\rho}\\
&-(c_2c_3m_2+c_3c_5d_2+c_2c_5d_3)\cos\pi\rho\cdot\xi^{2\rho}-d_2d_3m_2\cos\frac{\pi\varrho}{2}\cdot\xi^{\varrho}\\
&-(c_3d_2m_2+c_2d_3m_2+c_5d_2d_3)\cos\frac{\pi\rho}{2}\cdot\xi^{\rho}-d_2d_3m_2,\\
\mathscr{P}_1^I=&-c_2c_3c_5\sin\frac{\pi}{2}(\varrho+3\rho)\cdot\xi^{\varrho+3\rho}-(c_2c_3m_2+c_3c_5d_2+c_2c_5d_3)\sin\frac{\pi}{2}(\varrho+2\rho)\cdot\xi^{\varrho+2\rho}\\
&-c_2c_3c_5\sin\frac{3\pi\rho}{2}\cdot\xi^{3\rho}-(c_3d_2m_2+c_2d_3m_2+c_5d_2d_3)\sin\frac{\pi}{2}(\varrho+\rho)\cdot\xi^{\varrho+\rho}\\
&-(c_2c_3m_2+c_3c_5d_2+c_2c_5d_3)\sin\pi\rho\cdot\xi^{2\rho}-d_2d_3m_2\sin\frac{\pi\varrho}{2}\cdot\xi^{\varrho}\\
&-(c_3d_2m_2+c_2d_3m_2+c_5d_2d_3)\sin\frac{\pi\rho}{2}\cdot\xi^{\rho},\\
\mathscr{P}_2^R=&-c_3c_6\cos\pi(\varrho+\rho)\cdot\xi^{2(\varrho+\rho)}-2c_3c_6\cos\pi(\frac{\varrho}{2}+\rho)\cdot\xi^{\varrho+2\rho}\\
&-(c_3m_3+c_6d_3)\cos\pi(\frac{\rho}{2}+\varrho)\cdot\xi^{2\varrho+\rho}-2(c_3m_3+c_6d_3)\cos\pi\frac{\varrho+\rho}{2}\cdot\xi^{\varrho+\rho}\\
&-d_3m_3\cos\pi\varrho\cdot\xi^{2\varrho}-c_3c_6\cos\pi\rho\cdot\xi^{2\rho}-2d_3m_3\cos\frac{\pi\varrho}{2}\cdot\xi^{\varrho}\\
&-(c_3m_3+c_6d_3)\cos\frac{\pi\rho}{2}\cdot\xi^{\rho}-d_3m_3,
\end{aligned}
$$

$$\begin{aligned}
\mathscr{P}_2^I =& -c_3c_6\sin\pi(\varrho+\rho)\cdot\xi^{2(\varrho+\rho)} - 2c_3c_6\sin\pi(\frac{\varrho}{2}+\rho)\cdot\xi^{\varrho+2\rho}\\
&-(c_3m_3+c_6d_3)\sin\pi(\frac{\rho}{2}+\varrho)\cdot\xi^{2\varrho+\rho} - 2(c_3m_3+c_6d_3)\sin\pi\frac{\varrho+\rho}{2}\cdot\xi^{\varrho+\rho}\\
&-d_3m_3\sin\pi\varrho\cdot\xi^{2\varrho} - c_3c_6\sin\pi\rho\cdot\xi^{2\rho} - 2d_3m_3\sin\frac{\pi\varrho}{2}\cdot\xi^{\varrho}\\
&-(c_3m_3+c_6d_3)\sin\frac{\pi\rho}{2}\cdot\xi^{\rho},\\
\mathscr{P}_4^R =& \cos 2\pi\varrho\cdot\xi^{4\varrho} + 4\cos\frac{3\pi\varrho}{2}\cdot\xi^{3\varrho} + 6\cos\pi\varrho\cdot\xi^{2\varrho} + 4\cos\frac{\pi\varrho}{2}\cdot\xi^{\varrho} + 1,\\
\mathscr{P}_4^I =& \sin 2\pi\varrho\cdot\xi^{4\varrho} + 4\sin\frac{3\pi\varrho}{2}\cdot\xi^{3\varrho} + 6\sin\pi\varrho\cdot\xi^{2\varrho} + 4\sin\frac{\pi\varrho}{2}\cdot\xi^{\varrho}.
\end{aligned}$$

The coefficient matrix of Eq. (3.5) can be conveniently articulated as

$$\eta = \begin{bmatrix} l_{11} & l_{12} & l_{13} & l_{14} & l_{15} & l_{16}\\ l_{21} & l_{22} & l_{23} & l_{24} & l_{25} & l_{26}\\ l_{31} & l_{32} & l_{33} & l_{34} & l_{35} & l_{36}\\ l_{41} & l_{42} & l_{43} & l_{44} & l_{45} & l_{46}\\ l_{51} & l_{52} & l_{53} & l_{54} & l_{55} & l_{56}\\ l_{61} & l_{62} & l_{63} & l_{64} & l_{65} & l_{66} \end{bmatrix}.$$

To ensure the existence and uniqueness of the solution to Eq. (3.5), we assume η is invertible. With this in place, $\cos\xi\tau$ and $\sin\xi\tau$ can be derived via Cramer's rule to further determine the bifurcation point with respect to τ, as detailed in [39].

$$\begin{cases} \cos\xi\tau = \dfrac{\Lambda_1}{|\eta|} = \hbar_1(\xi),\\ \sin\xi\tau = \dfrac{\Lambda_2}{|\eta|} = \hbar_2(\xi), \end{cases} \tag{3.6}$$

where

$$\Lambda_1 = \begin{vmatrix} -\mathscr{P}_1^R & l_{12} & l_{13} & l_{14} & l_{15} & l_{16}\\ -\mathscr{P}_1^I & l_{22} & l_{23} & l_{24} & l_{25} & l_{26}\\ -\mathscr{P}_2^R & l_{32} & l_{33} & l_{34} & l_{35} & l_{36}\\ -\mathscr{P}_2^I & l_{42} & l_{43} & l_{44} & l_{45} & l_{46}\\ 0 & l_{52} & l_{53} & l_{54} & l_{55} & l_{56}\\ 0 & l_{62} & l_{63} & l_{64} & l_{65} & l_{66} \end{vmatrix}, \Lambda_2 = \begin{vmatrix} l_{11} & -\mathscr{P}_1^R & l_{13} & l_{14} & l_{15} & l_{16}\\ l_{21} & -\mathscr{P}_1^I & l_{23} & l_{24} & l_{25} & l_{26}\\ l_{31} & -\mathscr{P}_2^R & l_{33} & l_{34} & l_{35} & l_{36}\\ l_{41} & -\mathscr{P}_2^I & l_{43} & l_{44} & l_{45} & l_{46}\\ l_{51} & 0 & l_{53} & l_{54} & l_{55} & l_{56}\\ l_{61} & 0 & l_{63} & l_{64} & l_{65} & l_{66} \end{vmatrix}.$$

By applying the Trigonometric Pythagorean identity to Eq. (3.6), we obtain

$$\hbar_1^2(\xi) + \hbar_2^2(\xi) = 1. \tag{3.7}$$

Subsequently, the critical frequency is computed using Eq. (3.7), while an explicit expression for the bifurcation critical point is derived from Eq. (3.6). The following assumption is critical to the effective execution of the above approach.

(**A**2) For $|\eta| \neq 0$, Eq. (3.7) has positive real roots.

Eq. (3.6) gives the general form of the critical delays as

$$\tau^{(n)} = \frac{1}{\xi}\left[\arccos\hbar_1(\xi) + 2n\pi\right], \quad n = 0, 1, 2, \ldots,$$

from which the bifurcation threshold τ_0 for τ-induced bifurcation is identified as

$$\tau_0 = \min\{\tau^{(n)}\}, \quad n = 0, 1, 2, \ldots. \tag{3.8}$$

For rigorous bifurcation condition analysis, the following assumption is required.

(**A3**) $\left.\frac{\Re(\mathscr{M}(i\xi))\cdot\Re(\mathscr{N}(i\xi))+\Im(\mathscr{M}(i\xi))\cdot\Im(\mathscr{N}(i\xi))}{\Re^2(\mathscr{N}(i\xi))+\Im^2(\mathscr{N}(i\xi))}\right|_{(\xi=\xi_0,\tau=\tau_0)} \neq 0$, where $\mathscr{M}(i\xi)$ and $\mathscr{N}(i\xi)$ are subject to Eq. (3.10). $\Re(z(\cdot))$ and $\Im(z(\cdot))$ correspond to the real and imaginary elements of $z(\cdot)$, respectively.

Lemma 3.1. *Let $s(\tau) = \sigma(\tau) + i\mu(\tau)$ be the root of Eq. (3.2) near $\tau = \tau_0$ complying with $\sigma(\tau_0) = 0$, $\mu(\tau_0) = \xi_0$, then the transversality condition is valid under (A3)*

$$\Re\left[\frac{\mathrm{d}s}{\mathrm{d}\tau}\right]\Big|_{(\xi=\xi_0,\tau=\tau_0)} \neq 0.$$

Proof. By differentiating both sides of Eq. (3.2) with respect to τ, it follows that

$$\begin{aligned}&\mathscr{P}_0'(s)\frac{\mathrm{d}s}{\mathrm{d}\tau} + \mathscr{P}_1'(s)\mathrm{e}^{s\tau}\frac{\mathrm{d}s}{\mathrm{d}\tau} + \mathscr{P}_1(s)\mathrm{e}^{s\tau}\left(\tau\frac{\mathrm{d}s}{\mathrm{d}\tau}+s\right) + \mathscr{P}_2'(s)\mathrm{e}^{2s\tau}\frac{\mathrm{d}s}{\mathrm{d}\tau} + \mathscr{P}_2(s)\mathrm{e}^{2s\tau}\left(2\tau\frac{\mathrm{d}s}{\mathrm{d}\tau}+2s\right)\\ &+ \mathscr{P}_4'(s)\mathrm{e}^{4s\tau}\frac{\mathrm{d}s}{\mathrm{d}\tau} + \mathscr{P}_4(s)\mathrm{e}^{4s\tau}\left(4\tau\frac{\mathrm{d}s}{\mathrm{d}\tau}+4s\right) = 0.\end{aligned} \tag{3.9}$$

Via Eq. (3.9), we can establish a clear computational process to

$$\frac{\mathrm{d}s}{\mathrm{d}\tau} = \frac{\mathscr{M}(s)}{\mathscr{N}(s)}, \tag{3.10}$$

where

$$\mathscr{M}(s) = -s\mathscr{P}_1(s)\mathrm{e}^{s\tau} - 2s\mathscr{P}_2(s)\mathrm{e}^{2s\tau} - 4s\mathscr{P}_4(s)\mathrm{e}^{4s\tau},$$

and

$$\mathscr{N}(s) = \mathscr{P}_0'(s) + \left(\mathscr{P}_1'(s) + \tau\mathscr{P}_1(s)\right)\mathrm{e}^{s\tau} + \left(\mathscr{P}_2'(s) + 2\tau\mathscr{P}_2(s)\right)\mathrm{e}^{2s\tau} + \left(\mathscr{P}_4'(s) + 4\tau\mathscr{P}_4(s)\right)\mathrm{e}^{4s\tau}.$$

Thus, by (**A**3) we can deduce from Eq. (3.10) that

$$\Re\left[\frac{\mathrm{d}s}{\mathrm{d}\tau}\right]\Big|_{(\xi=\xi_0,\tau=\tau_0)} = \left.\frac{\Re(\mathscr{M}(i\xi))\cdot\Re(\mathscr{N}(i\xi))+\Im(\mathscr{M}(i\xi))\cdot\Im(\mathscr{N}(i\xi))}{\Re^2(\mathscr{N}(i\xi))+\Im^2(\mathscr{N}(i\xi))}\right|_{(\xi=\xi_0,\tau=\tau_0)} \neq 0.$$

Accordingly, the transversality is in effect. □

We now state the main theorem.

Theorem 3.2. *Under (A1)-(A3), the following holds for FONTRNN (2.3):*
(1) The origin is asymptotically stable for all $\tau \in [0, \tau_0)$.
(2) A Hopf bifurcation occurs from the origin as τ crosses τ_0.

Remark 3.3. The characteristic equation (3.2) involves three distinct orders of transcendental terms, with the highest-order term being $e^{4s\tau}$. This differs from the scenarios in existing literature: [15] directly separates the real and imaginary parts to solve for $\cos\xi\tau$, which is inapplicable here due to the lack of high-order transcendental terms in their model; while [31] deals with three transcendental terms with a maximum order of $e^{3s\tau}$ via two-step order reduction for the joint solution of $\cos\xi\tau$. To address this challenge, we adopt an order reduction and

dimension augmentation approach: first, multiply both sides of (3.2) by $e^{-s\tau}$, $e^{-2s\tau}$, and $e^{-3s\tau}$ respectively to convert the original equation into three equations with low-order transcendental terms; second, expand these equations into a linear system of trigonometric variables in terms of $\xi\tau$; finally, solve for $\cos\xi\tau$ using Cramer's rule.

Remark 3.4. Under Assumption **A**1, if Assumption **A**2 is violated (i.e., Eq. (3.7) has no positive real roots), then the characteristic equation $\det(\Delta(s)) = 0$ possesses no purely imaginary roots for any delay parameter $\tau > 0$. By Theorem 3.3 in [40], the equilibrium of system (2.3) remains asymptotically stable for all $\tau > 0$. This implies that Assumption **A**2 is essential to induce bifurcations or instability.

3.2. **Neutral term order induced bifurcation in FONTRNN.** Next, we proceed to analyze the Hopf bifurcation induced by the neutral term order ρ in network (2.3). Our analysis is based on the functions $\Gamma_1(\xi,\rho)$ and $\Gamma_2(\xi,\rho)$ from Eq. (3.5)

$$\Gamma_1(\xi,\rho) = \mathscr{P}_1^R\cos\xi\tau + \mathscr{P}_1^I\sin\xi\tau + \left(\mathscr{P}_0^R + \mathscr{P}_4^R\right)\cos 2\xi\tau + \left(\mathscr{P}_0^I - \mathscr{P}_4^I\right)\sin 2\xi\tau + \mathscr{P}_2^R, \tag{3.11}$$

and

$$\Gamma_2(\xi,\rho) = \mathscr{P}_1^I\cos\xi\tau - \mathscr{P}_1^R\sin\xi\tau + \left(\mathscr{P}_0^I + \mathscr{P}_4^I\right)\cos 2\xi\tau + \left(\mathscr{P}_4^R - \mathscr{P}_0^R\right)\sin 2\xi\tau + \mathscr{P}_2^I. \tag{3.12}$$

To ensure the meaningfulness of our study, we assume the existence of at least one intersection point $N_n(\xi_n,\rho_n)$ between the curves $\Gamma_1(\xi,\rho)$ and $\Gamma_2(\xi,\rho)$. This assumption allows the range of such points to be determined graphically. We then numerically solve for the specific coordinates of $N_n(\xi_n,\rho_n)$ within the specified domain using an implicit function array command in Maple. The critical bifurcation parameter is defined as

$$\tilde{\rho}_0 = \min(\rho_n), n = 1,2,3,\cdots \tag{3.13}$$

along with the corresponding value $\tilde{\xi}_0$ from the pair $N_n(\xi_n,\rho_n)$.

For the Hopf bifurcation transversality condition, the following assumption is required.

(**A**4) $\left.\frac{\Re(\tilde{\mathscr{M}}(i\xi))\cdot\Re(\tilde{\mathscr{N}}(i\xi))+\Im(\tilde{\mathscr{M}}(i\xi))\cdot\Im(\tilde{\mathscr{N}}(i\xi))}{\Re^2(\tilde{\mathscr{N}}(i\xi))+\Im^2(\tilde{\mathscr{N}}(i\xi))}\right|_{(\xi=\tilde{\xi}_0,\rho=\tilde{\rho}_0)} \neq 0$, where $\tilde{\mathscr{M}}(i\xi)$ and $\tilde{\mathscr{N}}(i\xi)$ are subject to Eq. (3.14).

Lemma 3.5. *Assume that $s(\rho) = \tilde{\sigma}(\rho) + i\tilde{\mu}(\rho)$ is the root of Eq. (3.2) near $\rho = \tilde{\rho}_0$ satisfying $\tilde{\sigma}(\tilde{\rho}_0) = 0$ and $\tilde{\mu}(\tilde{\rho}_0) = \tilde{\xi}_0$. Then the transversality condition holds under assumption (A4)*

$$\Re\left[\frac{ds}{d\rho}\right]\Bigg|_{(\xi=\tilde{\xi}_0,\rho=\tilde{\rho}_0)} \neq 0.$$

Proof. Differentiating both sides of Eq. (3.2) with respect to ρ yields a well-defined computational procedure to

$$\frac{ds}{d\rho} = \frac{\tilde{\mathscr{M}}(s)}{\tilde{\mathscr{N}}(s)}, \tag{3.14}$$

where

$$\tilde{\mathscr{M}}(s) = \left(\Sigma_3 e^{2s\tau} + \Sigma_4 e^{s\tau} + \Sigma_6\right) s^\rho ln(s),$$

and

$$\tilde{\mathscr{N}}(s) = 4(s^{\varrho}+1)^3\Sigma_1 e^{4s\tau} - \left(\rho s^{\rho-1}\Sigma_3 + 2\Sigma_1\Sigma_2\right)e^{2s\tau} - \left(\rho s^{\rho-1}\Sigma_4 + \Sigma_1\Sigma_5\right)e^{s\tau} - \rho s^{\rho-1}\Sigma_6,$$

where

$$\begin{aligned}
\Sigma_1 &= \varrho s^{\varrho-1} + \tau(s^{\varrho}+1), \Sigma_2 = (s^{\varrho}+1)(c_3 s^{\rho}+d_3)(c_6 s^{\rho}+m_3),\\
\Sigma_3 &= (s^{\varrho}+1)^2\left((c_3 s^{\rho}+d_3)c_6 + (c_6 s^{\rho}+m_3)c_3\right),\\
\Sigma_4 &= (s^{\varrho}+1)\left((c_2 s^{\rho}+d_2)(c_3 s^{\rho}+d_3)c_5 + (c_2 s^{\rho}+d_2)(c_5 s^{\rho}+m_2)c_3 + (c_3 s^{\rho}+d_3)(c_5 s^{\rho}+m_2)c_2\right),\\
\Sigma_5 &= (c_2 s^{\rho}+d_2)(c_3 s^{\rho}+d_3)(c_5 s^{\rho}+m_2),\\
\Sigma_6 &= (c_1 s^{\rho}+d_1)(c_2 s^{\rho}+d_2)(c_3 s^{\rho}+d_3)c_4 + (c_1 s^{\rho}+d_1)(c_2 s^{\rho}+d_2)(c_4 s^{\rho}+m_1)c_3\\
&\quad + (c_1 s^{\rho}+d_1)(c_3 s^{\rho}+d_3)(c_4 s^{\rho}+m_1)c_2 + (c_2 s^{\rho}+d_2)(c_3 s^{\rho}+d_3)(c_4 s^{\rho}+m_1)c_1.
\end{aligned}$$

Thus, by (**A**4), we can deduce from Eq. (3.14) that

$$\Re\left[\frac{ds}{d\rho}\right]\Big|_{(\xi=\tilde{\xi}_0,\rho=\tilde{\rho}_0)} = \frac{\Re(\tilde{\mathscr{M}}(i\xi))\cdot\Re(\tilde{\mathscr{N}}(i\xi)) + \Im(\tilde{\mathscr{M}}(i\xi))\cdot\Im(\tilde{\mathscr{N}}(i\xi))}{\Re^2(\tilde{\mathscr{N}}(i\xi)) + \Im^2(\tilde{\mathscr{N}}(i\xi))}\Big|_{(\xi=\tilde{\xi}_0,\rho=\tilde{\rho}_0)} \neq 0.$$

Accordingly, the transversality is in effect. □

To determine the stability interval of the system with respect to parameter ρ, we need to further analyze the boundary case where the neutral term order $\rho = 0$. To this end, we substitute $\rho = 0$ into the characteristic equation, reducing it to the form defined by Eqs. (3.11) and (3.12)

$$\begin{cases}
\bar{\mathscr{P}}_1^R\cos\xi\tau + \bar{\mathscr{P}}_1^I\sin\xi\tau + \left(\bar{\mathscr{P}}_0^R + \bar{\mathscr{P}}_4^R\right)\cos 2\xi\tau - \bar{\mathscr{P}}_4^I\sin 2\xi\tau + \bar{\mathscr{P}}_2^R = 0,\\
\bar{\mathscr{P}}_1^I\cos\xi\tau - \bar{\mathscr{P}}_1^R\sin\xi\tau + \bar{\mathscr{P}}_4^I\cos 2\xi\tau + \left(\bar{\mathscr{P}}_4^R - \bar{\mathscr{P}}_0^R\right)\sin 2\xi\tau + \bar{\mathscr{P}}_2^I = 0,
\end{cases} \tag{3.15}$$

where $\mathscr{P}_J^R\big|_{\rho=0} = \bar{\mathscr{P}}_J^R, \mathscr{P}_J^I\big|_{\rho=0} = \bar{\mathscr{P}}_J^I, J = 0,1,2,4.$

Lemma 3.6. *The system (2.3) is asymptotically stable at the origin if the following conditions hold for the case where $\rho = 0$:*

(1) $C_0, C_1 > 0, 4C_2 > C_1$, and $C_1(4C_2 - C_1) > 16C_0$,
(2) Eq. (3.15) has no real roots in ξ.

Proof. For the system (2.3) with a degenerate neutral term, when $\tau = 0$, the characteristic equation can be rewritten as:

$$s^{4\varrho} + 4s^{3\varrho} + C_2 s^{2\varrho} + C_1 s^{\varrho} + C_0 = 0,$$

where

$$\begin{aligned}
C_0 &= 1 - (c_3+d_3)[(c_6+m_3) + (c_2+d_2)((c_5+m_2) + (c_1+d_1)(c4+m_1))],\\
C_1 &= 4 - 2(c_3+d_3)(c_6+m_3) - (c_2+d_2)(c_3+d_3)(c_5+m_2),\\
C_2 &= 6 - (c_3+d_3)(c_6+m_3).
\end{aligned}$$

Applying the Routh-Hurwitz criterion for fractional-order systems reveals that when the determinants satisfy $C_0, C_1 > 0$, $4C_2 > C_1$, and $C_1(4C_2 - C_1) > 16C_0$, all characteristic roots possess negative real parts. Following Lemma 2.2, this condition guarantees the asymptotic stability of system (2.3) at $\tau = 0$.

Furthermore, for any $\tau > 0$, the characteristic equation of system (2.3) with $\rho = 0$ exhibits no purely imaginary roots. Consequently, by Corollary 3 in [41], the trivial solution of this reduced system remains stable for all $\tau > 0$. □

Theorem 3.7. *If Assumptions **A1**, **A4** and Lemma 3.6 hold, then the following results hold:*
(1) The origin of FONTRNN (2.3) is asymptotically stable for all ρ in $[0,\rho_0)$.
(2) A Hopf bifurcation occurs at the origin of the FONTRNN (2.3) when $\rho=\rho_0$.

Remark 3.8. In contrast to the analytical approach in [25–27], which determines the stability interval for a bifurcation parameter near zero via a degenerate form such as Lemma 3.5, our method must account for an essential structural difference. When $\rho=0$, the system retains the fractional derivative order ϱ, leading to a characteristic equation that cannot be decoupled or explicitly resolved in the same manner. As a result, solutions in the sense of prior literature may not exist in this context. To address this, we instead analyze the degenerate system directly. By combining the Routh–Hurwitz criterion for fractional-order systems with continuity arguments, we establish stability at $\rho=0$, thereby completing the derivation of the bifurcation theorem with respect to the neutral term order.

4. Numerical Verifications

Three representative examples are presented in this section to numerically validate the occurrence of both delay-induced and neutral-term-order-induced Hopf bifurcations, utilizing the Adams-type predictor-corrector method [42] for accurate simulations.

4.1. **Example 1.** We consider the FONTRNN model (2.3) with the following parameter set:

$$\begin{cases} D^{0.96}u_1(t) = -u_1(t)+\tanh(u_2(t-\tau))+0.4D^{0.93}u_2(t-\tau),\\ D^{0.96}u_2(t) = -u_2(t)+\tanh(u_3(t-\tau))+0.6D^{0.93}u_3(t-\tau),\\ D^{0.96}u_3(t) = -u_3(t)+\tanh(u_4(t-\tau))+0.3D^{0.93}u_4(t-\tau),\\ D^{0.96}u_4(t) = -u_4(t)-0.8\tanh(u_1(t-\tau))-0.8\tanh(u_2(t-\tau))-0.8\tanh(u_3(t-\tau))\\ \qquad\qquad -0.5D^{0.93}u_1(t-\tau)-0.4D^{0.93}u_2(t-\tau)+0.6D^{0.93}u_3(t-\tau). \end{cases} \tag{4.1}$$

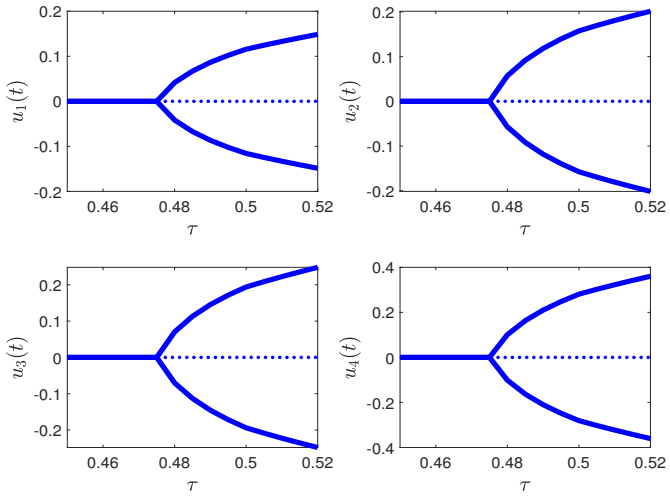

FIGURE 1. Bifurcation diagrams driven by τ for FONTRNN (4.1).

The initial values are selected as $u_1(0) = 0.08$, $u_2(0) = 0.06$, $u_3(0) = 0.08$, and $u_4(0) = 0.06$. Applying the analytical framework established in Section 3.1, we compute the critical frequency $\xi_0 \approx 1.1578$ and critical delay $\tau_0 \approx 0.4754$ for system (4.1). The positive transversality condition $\Re[\mathrm{d}s/\mathrm{d}\tau]|_{(\xi=1.1578,\tau=0.4754)} \approx 0.552 > 0$ confirms the existence of a Hopf bifurcation at $\tau = \tau_0$, consistent with Theorem 3.2. Fig. 1 displays the bifurcation diagram with respect to the delay parameter τ, confirming the existence of the Hopf bifurcation at $\tau = \tau_0$. To probe the dynamical regimes separated by this critical threshold, we analyze time responses and phase trajectories, which reveal distinct behaviors: for $\tau = 0.45 < \tau_0$ the time responses in Fig. 2 exhibits exponentially decaying characteristics, and the phase trajectory in Fig. 3 converges to the origin, confirming the asymptotic stability of the equilibrium point. When the delay exceeds the critical threshold $\tau = 0.50 > \tau_0$, Figs. 4, 5 demonstrate the instability of the origin.

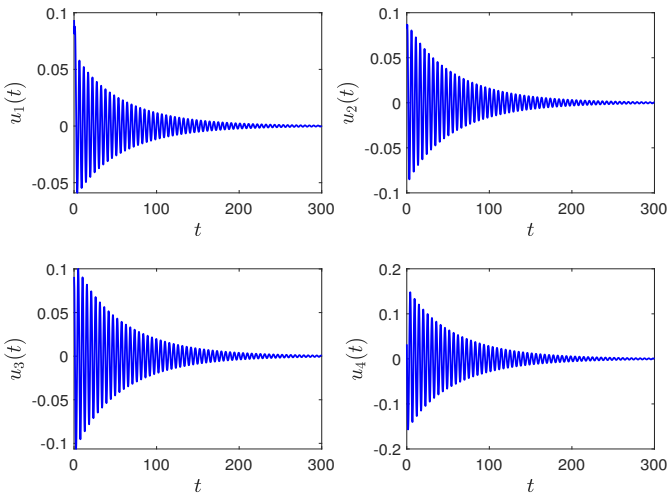

FIGURE 2. Time responses of FONTRNN (4.1) with $\tau = 0.45 < \tau_0 \approx 0.4754$.

To systematically assess the stability of the FONTRNN (4.1), we mapped the Hopf bifurcation critical delay τ_0 across the parameter space ϱ, ρ. Fig. 6 presents a heatmap illustrating the bifurcation critical value τ_0 over the parameter space $\varrho, \rho \in [0.5, 1]$. The color bar reflects the magnitude of τ_0, with warmer colors indicate lower critical values, while cooler colors correspond to higher ones. Based on Theorem 3.2, a smaller τ_0 indicates reduced stability, making the system prone to instability under smaller delays, while a larger τ_0 enhances stability robustness, maintaining system performance over a wider range of time delays. Clearly, τ_0 decreases as ϱ increases, revealing a destabilizing effect of ϱ. Conversely, τ_0 increases with ρ, indicating that ρ plays a stabilizing role. These results highlight the distinct and opposing influences of ϱ and ρ on the delay-induced stability of the system.

To quantify the parametric sensitivity of the critical delay threshold τ_0, we employ the Normalized Forward Sensitivity Index (NFSI) here [43]. For a parameter θ, the NFSI is defined as:

$$S(\tau_0, \theta) = \frac{\partial \tau_0}{\partial \theta} \cdot \frac{\theta}{\tau_0}. \tag{4.2}$$

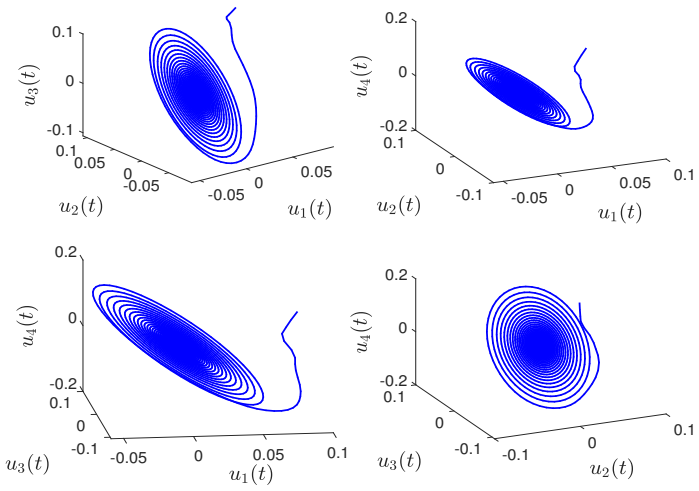

FIGURE 3. Phase trajectories of FONTRNN (4.1) with $\tau = 0.45 < \tau_0 \approx 0.4754$.

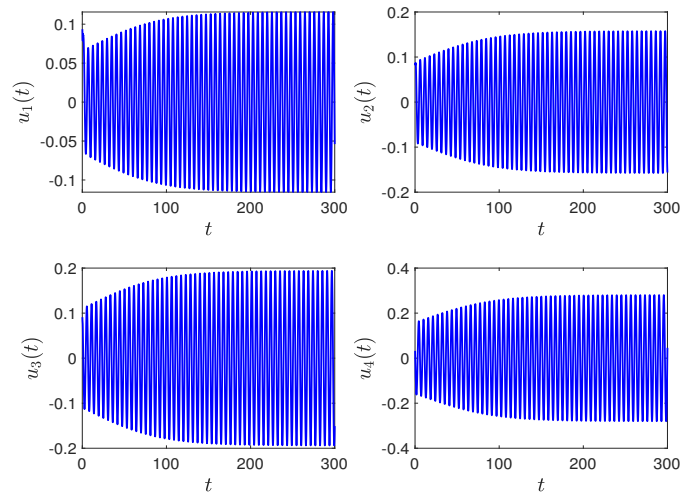

FIGURE 4. Time responses of FONTRNN (4.1) with $\tau = 0.50 > \tau_0 \approx 0.4754$.

However, due to the transcendental nature of Eq. (3.7), which precludes closed-form solutions for $\tau_0(\theta)$, we adopt the central difference scheme to approximate the partial derivatives. By defining $\varepsilon = r\theta$ $(r \ll 1)$, the sensitivity calculation simplifies to

$$S(\tau_0,\theta) = \frac{\tau_0(\theta+\varepsilon)-\tau_0(\theta-\varepsilon)}{2\varepsilon}\cdot\frac{\theta}{\tau_0} = \frac{\tau_0((1+r)\theta)-\tau_0((1-r)\theta)}{2\tau_0(\theta)}.$$

At $r = 0.01$, the sensitivity indices, presented as a bar chart in Fig. 7, reveal distinct contributions: fractional derivative order ϱ exerts the strongest negative influence on τ_0, while the neutral-type fractional order ρ exhibits the largest positive effect. Among other parameters, a_3 also demonstrates a notable negative contribution. These findings align with the heatmap in Fig. 6, where spatial intensity variations corroborate the opposing roles of fractional orders on τ_0.

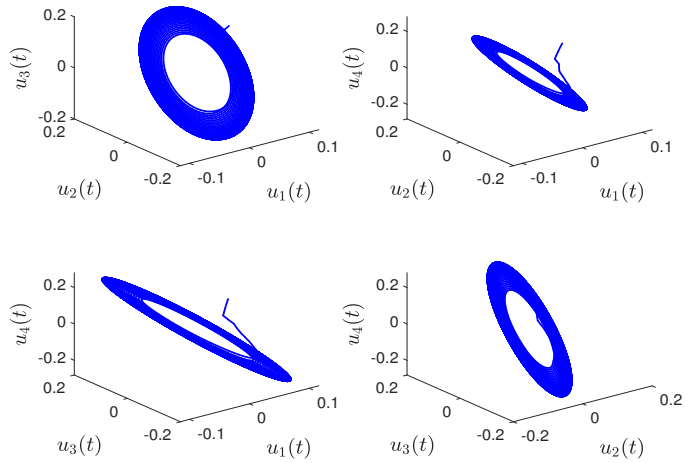

FIGURE 5. Phase trajectories of FONTRNN (4.1) with $\tau = 0.50 > \tau_0 \approx 0.4754$.

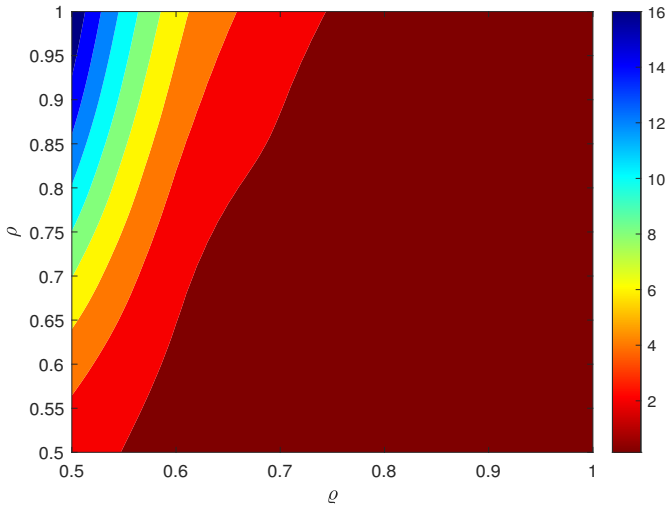

FIGURE 6. Bifurcation critical value τ_0 heatmap with$\varrho, \rho \in [0.5, 1]$.

where antagonistic intensity variations of ϱ and ρ corroborate their opposing regulatory roles. The remaining parameters show negligible sensitivity indices, indicating minimal impact on the critical delay.

Remark 4.1. The absence of a closed-form expression for the frequency parameter ξ necessitates numerical computation of τ_0 by solving the implicit $\xi - \tau^{(n)}$ relationship. This implicit dependency, coupled with the parameter-sensitive variability of ξ, precludes a unified analytical form for τ_0 and renders conventional derivative-based sensitivity analysis infeasible. We therefore employ a central difference scheme to compute normalized sensitivity indices. The $\mathscr{O}(\varepsilon^2)$ truncation error of this approximation is rigorously bounded via second-order Taylor expansion, ensuring robust sensitivity ranking—a critical requirement for identifying dominant stability regulators in fractional-order delay systems.

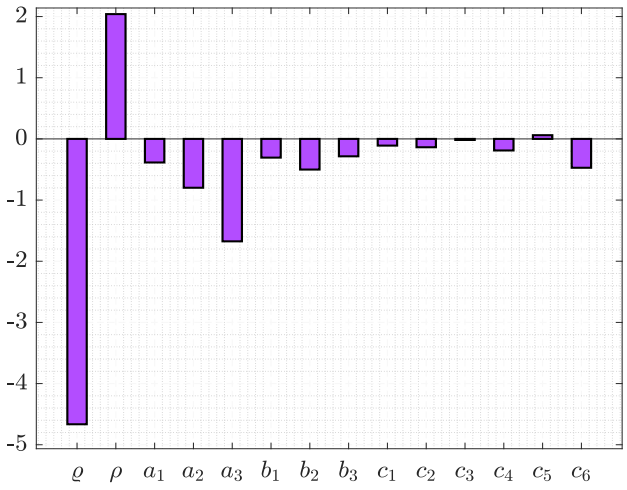

FIGURE 7. Parameter sensitivity analysis of FONTRNN (4.1).

4.2. **Example 2.** In this example, we select the parameters:

$$\begin{cases} D^{0.92}u_1(t) = -u_1(t) + 0.8\tanh(u_2(t-\tau)) - 0.4D^{0.86}u_2(t-\tau), \\ D^{0.92}u_2(t) = -u_2(t) + 0.9\tanh(u_3(t-\tau)) - 0.5D^{0.86}u_3(t-\tau), \\ D^{0.92}u_3(t) = -u_3(t) + \tanh(u_4(t-\tau)) - 0.5D^{0.86}u_4(t-\tau), \\ D^{0.92}u_4(t) = -u_4(t) + 1.2\tanh(u_1(t-\tau)) + 1.3\tanh(u_2(t-\tau)) - 1.4\tanh(u_3(t-\tau)) \\ \qquad\qquad - 0.3D^{0.86}u_1(t-\tau) - 0.3D^{0.86}u_2(t-\tau) - 0.6D^{0.86}u_3(t-\tau). \end{cases} \tag{4.3}$$

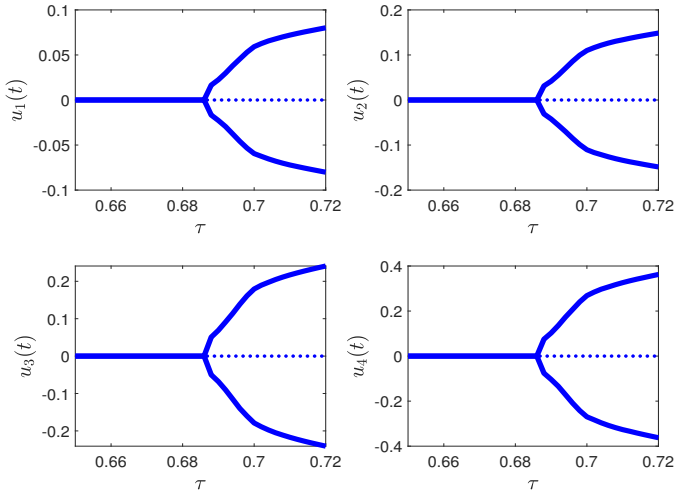

FIGURE 8. Bifurcation diagrams driven by τ for FONTRNN (4.3).

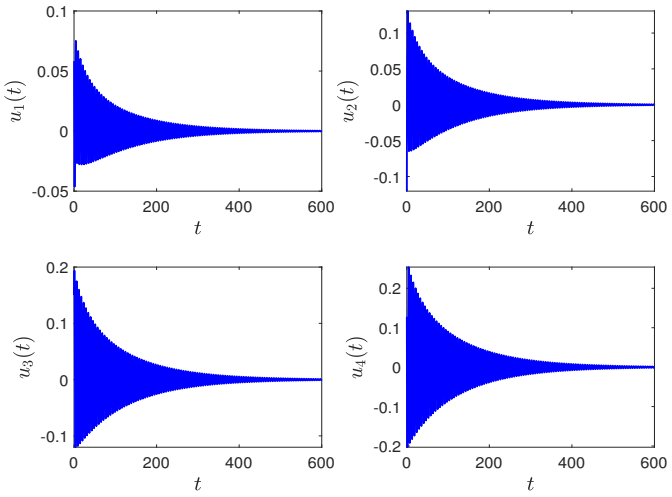

FIGURE 9. Time responses of FONTRNN (4.3) with $\tau = 0.64 < \tau_0 \approx 0.6869$.

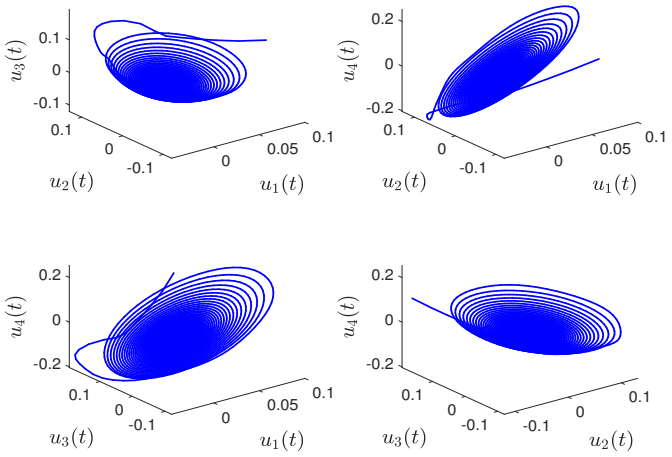

FIGURE 10. Phase trajectories of FONTRNN (4.3) with $\tau = 0.64 < \tau_0 \approx 0.6869$.

The initial values are selected as $u_1(0) = 0.05,\ u_2(0) = -0.1,\ u_3(0) = 0.18,\ u_4(0) = 0.2$. The critical delay is calculated as $\tau_0 \approx 0.6869$. Fig. 8 shows the bifurcation diagram, which confirms the Hopf bifurcation at $\tau = \tau_0$. For $\tau = 0.64 < \tau_0$, the time responses in Fig. 9 and the phase trajectories in Fig. 10 demonstrate that the system is asymptotically stable. However, when $\tau = 0.70 > \tau_0$, Figs. 11 and 12 exhibit oscillations, verifying stability loss.

The heatmap in Fig. 13 illustrates the joint effect of ϱ and ρ on τ_0. In contrast to Example 4.1, both fractional orders here have a negative correlation with τ_0: decreasing either ϱ or ρ increases the critical delay, thereby enhancing stability. This result highlights the flexibility of fractional-order models in tuning stability margins, a feature not achievable in integer-order networks.

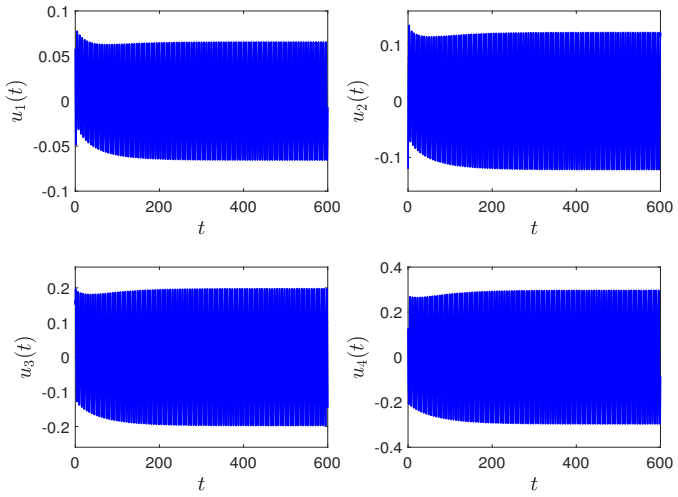

FIGURE 11. Time responses of FONTRNN (4.3) with $\tau = 0.7 > \tau_0 \approx 0.6869$.

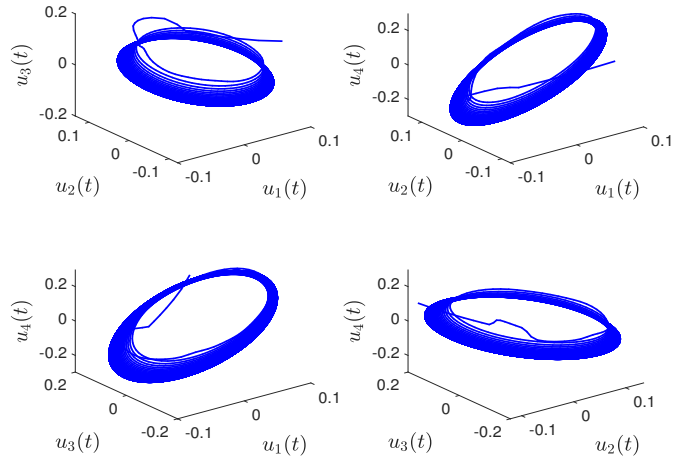

FIGURE 12. Phase trajectories of FONTRNN (4.3) with $\tau = 0.7 > \tau_0 \approx 0.6869$.

The quantitative sensitivity analysis in Fig.14 reveals that the fractional derivative order ϱ exerts by far the dominant influence on the critical delay τ_0, while the neutral term order ρ remains a non-negligible contributing factor, albeit secondary in magnitude.

Remark 4.2. In Example 4.2, both the fractional derivative order ϱ and the neutral term order ρ exhibit a synergistic effect on the bifurcation threshold τ_0. This behavior can be attributed to the sign consistency in the coefficients of the neutral and derivative terms when rearranged algebraically. Although both orders influence the stability in the same direction, the derivative order ϱ has a stronger effect than the neutral order ρ. In more general cases, such as Example 4.1, the role of neutral term coefficients and their interaction with fractional orders may lead to more complex behavior, warranting further investigation.

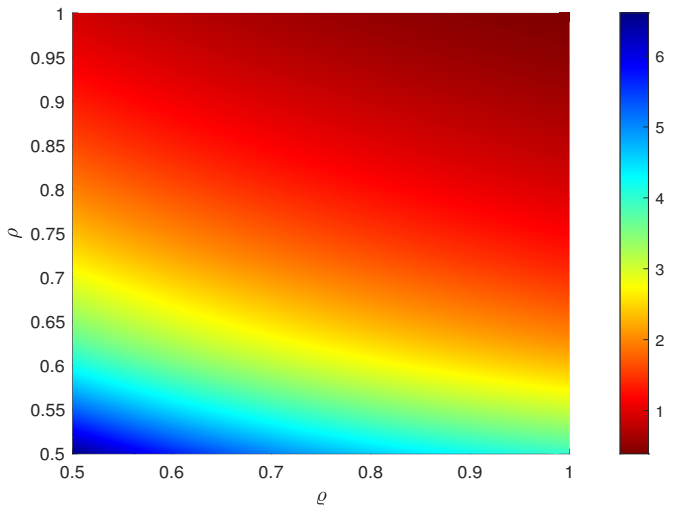

FIGURE 13. Bifurcation critical value τ_0 heatmap with $\varrho, \rho \in [0.5, 1]$.

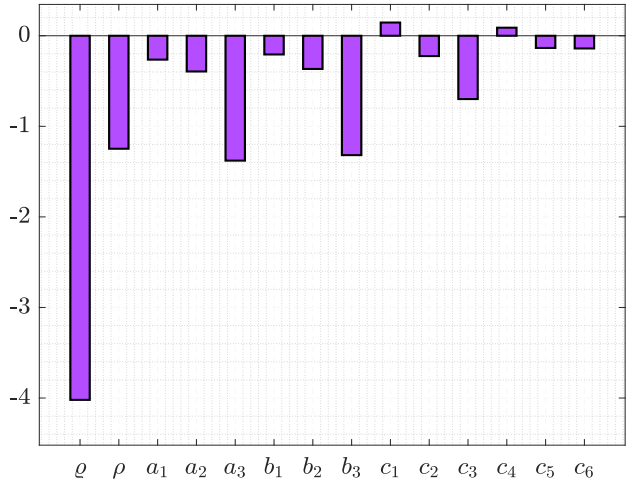

FIGURE 14. Parameter sensitivity analysis of FONTRNN (4.3).

4.3. **Example 3.** In this example, we select the parameters:

$$\begin{cases} D^{0.96}u_1(t) = -u_1(t) + \tanh(u_2(t-\tau)) + 0.5D^{\rho}u_2(t-\tau), \\ D^{0.96}u_2(t) = -u_2(t) + \tanh(u_3(t-\tau)) + 0.4D^{\rho}u_3(t-\tau), \\ D^{0.96}u_3(t) = -u_3(t) + 0.9\tanh(u_4(t-\tau)) + 0.6D^{\rho}u_4(t-\tau), \\ D^{0.96}u_4(t) = -u_4(t) - 0.9\tanh(u_1(t-\tau)) - 0.8\tanh(u_2(t-\tau)) - 0.8\tanh(u_3(t-\tau)) \\ \qquad\qquad - 0.8D^{\rho}u_1(t-\tau) - 0.7D^{\rho}u_2(t-\tau) - 0.2D^{\rho}u_3(t-\tau). \end{cases} \tag{4.4}$$

The initial values are selected as $u_1(0) = 0.01,\ u_2(0) = 0.01,\ u_3(0) = 0.01,\ u_4(0) = 0.01$.

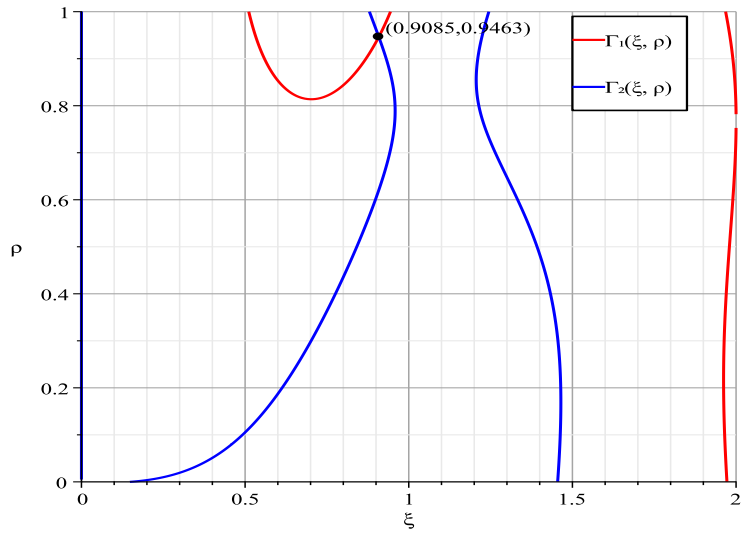

FIGURE 15. Intersection graph of ξ vs ρ for FONTRNN (4.4) with $\tau = 0.9$.

When $\tau = 0.9$ we can draw the intersection diagram according to the implicit function group, as shown in Fig. 15. Using Maple, we obtain $\tilde{\xi}_0 \approx 0.9085, \rho_0 \approx 0.9463, C_0 = 9.475, C_1 = 10.15, C_2 = 7.5$ and $\Re\left[\frac{ds}{d\rho}\right]\Big|_{(\xi=\tilde{\xi}_0,\rho=\tilde{\rho}_0)} \approx 0.089 \neq 0$. It is also straightforward to verify that the conditions in Theorem 3.7 are satisfied. Fig. 16 shows the bifurcation diagram, which confirms the Hopf bifurcation at $\rho = \rho_0$. For $\rho = 0.92 < \rho_0$, the time responses in Fig. 17 and phase trajectories in Fig. 18 demonstrate that the system is asymptotically stable. However, when $\rho = 0.97 > \rho_0$, Figs. 19 and 20 show oscillatory behavior, confirming the loss of stability.

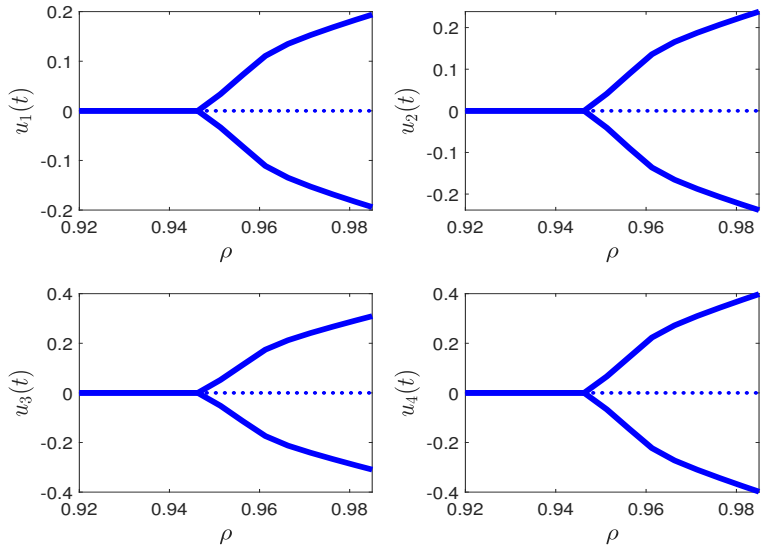

FIGURE 16. Bifurcation diagrams driven by ρ for FONTRNN (4.4).

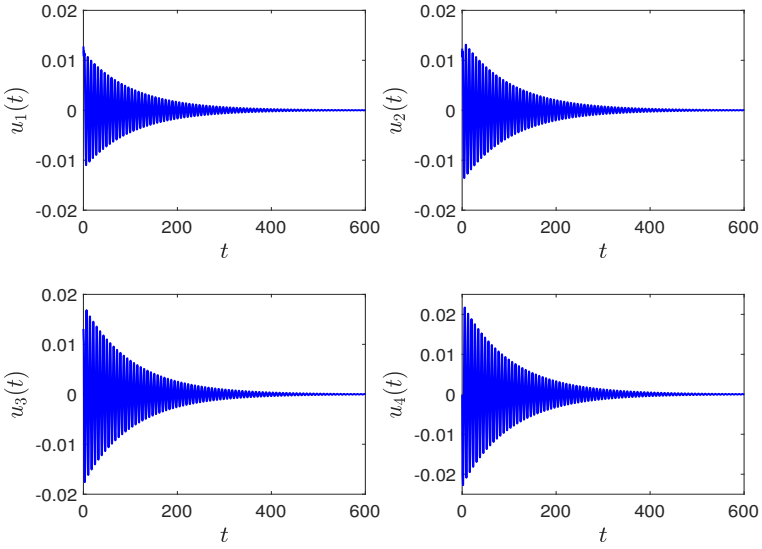

FIGURE 17. Time responses of FONTRNN (4.4) with $\rho = 0.92 < \rho_0 \approx 0.9463$.

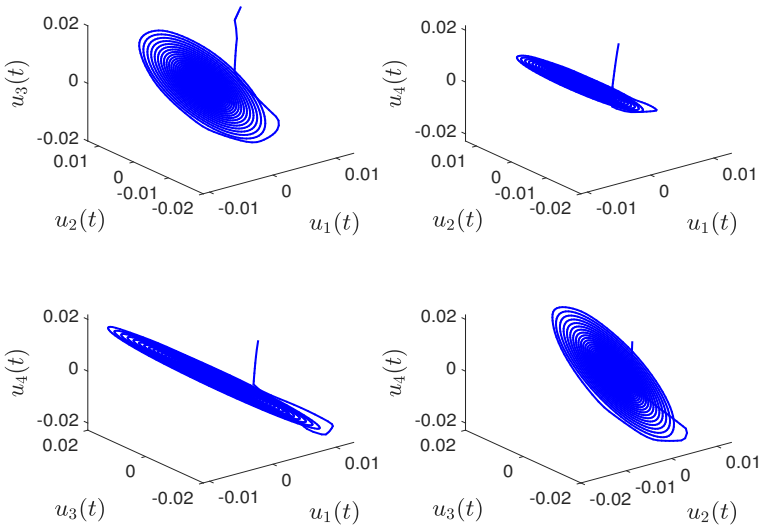

FIGURE 18. Phase trajectories of FONTRNN (4.4) with $\rho = 0.92 < \rho_0 \approx 0.9463$.

5. CONCLUSIONS

This study establishes a comprehensive theoretical framework for analyzing stability and bifurcation dynamics in high-dimensional fractional-order neutral-type delayed neural networks (FONTRNNs) with independently adjustable orders. By integrating dimensional elevation, Cramer's rule, and implicit function curve intersection methods, we successfully overcome the computational challenges posed by high-order transcendental equations in neutral-type systems, enabling precise determination of Hopf bifurcation thresholds for two distinct types of parameters.

Our investigation of delay-induced bifurcation demonstrates that time delay serves as a crucial regulatory factor for system stability. When delay exceeds its critical threshold, it triggers

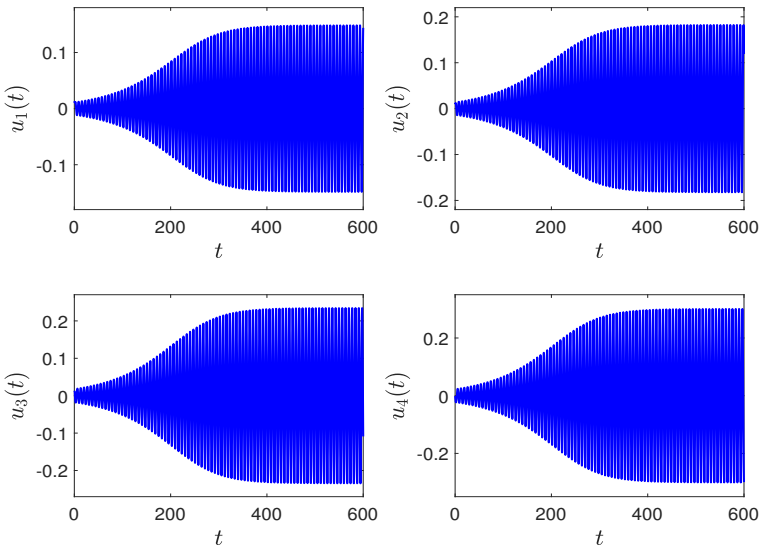

FIGURE 19. Time responses of FONTRNN (4.4) with $\rho = 0.97 > \rho_0 \approx 0.9463$.

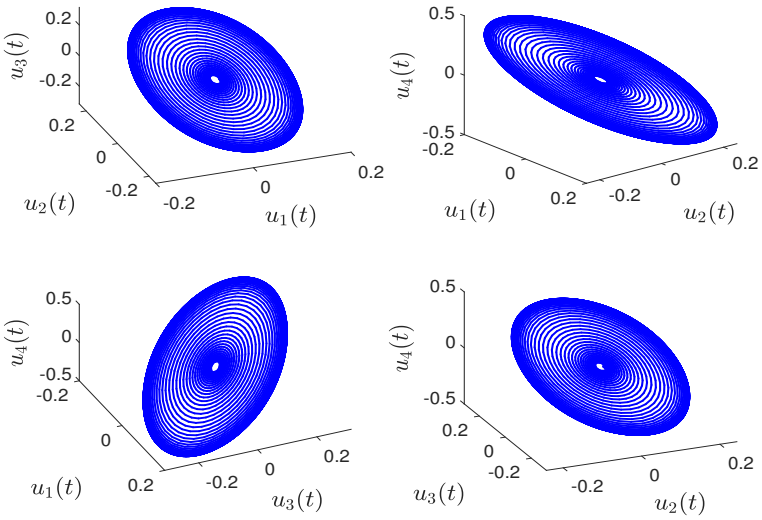

FIGURE 20. Phase trajectories of FONTRNN (4.4) with $\rho = 0.97 > \rho_0 \approx 0.9463$.

Hopf bifurcation, leading to sustained oscillations in the system. More significantly, we reveal that the two core parameters of the fractional-order system—the derivative order and the neutral term order—exert significant yet opposing effects on the bifurcation threshold. An increase in ϱ reduces the stability threshold and weakens system stability, whereas an increase in ρ can either enhance or diminish system robustness, depending on specific parametric conditions. The neutral term order-induced bifurcation analysis further reveals that, for a fixed time delay, the neutral term order itself can serve as an independent bifurcation parameter regulating system dynamics. Once the neutral term order surpasses its critical value, the system transitions from a stable state to an unstable one. This finding opens a new avenue for the dynamic control of system stability.

The proposed framework offers substantial application potential across multiple domains. In neuromorphic computing, independent order adjustment enables enhanced flexibility for implementing frequency-adaptive neural oscillators. For biological neural modeling, this approach permits more accurate representation of diverse neural processes characterized by distinct memory properties. Furthermore, in secure communication systems, the rich dynamics generated by order variations provide new opportunities for designing complex encryption signals. Based on the results of this study, we outline two directions for future research: (1) Extend the current model to investigate bifurcations in FONTRNNs with heterogeneous neutral delays and independently tunable fractional orders across network nodes. (2) Systematically characterize the parametric conditions that determine whether increasing the neutral-term fractional order stabilizes or destabilizes the system dynamics.

Acknowledgements

This paper was supported by Natural Science Foundation of Hunan Province under (No. 2022JJ 30271, 2024JJ7203), the key Project of Hunan Provincial Education Department (No. 23A0577), Yongzhou City Guided Science and Technology Plan Project (No. 2023YZ002) and Hunan University of Science and Engineering Research Project (No. 23XKYZZ05).

REFERENCES

[1] V. P. Dubey, J. Singh, A. M. Alshehri, S. Dubey, D. Kumar, Numerical investigation of fractional model of phytoplankton–toxic phytoplankton–zooplankton system with convergence analysis, International Journal of Biomathematics 15 (2022) 2250006.

[2] T. J. Anastasio, The fractional-order dynamics of brainstem vestibulo-oculomotor neurons, Biological Cybernetics 72 (1994) 69–79.

[3] T. J. Freeborn, A survey of fractional-order circuit models for biology and biomedicine, IEEE Journal on Emerging and Selected Topics in Circuits and Systems 3 (2013) 416–424.

[4] D. Kumar, J. Singh, Fractional Calculus in Medical and Health Science, CRC Press, 2020.

[5] Z. Sabir, S. B. Said, Q. Al-Mdallal, A fractional order numerical study for the influenza disease mathematical model, Alexandria Engineering Journal 65 (2023) 615–626.

[6] C. Pleumpreedaporn, S. Pleumpreedaporn, C. Thaiprayoon, J. Kongson, W. Sudsutad, Numerical simulation and analysis for variable-order fractal-fractional derivatives of bio-ethanol production models with recycling and death rate effects, Journal of Nonlinear Functional Analysis 2025 (2025) 12.

[7] A. S. Elwakil, Fractional-order circuits and systems: An emerging interdisciplinary research area, IEEE Circuits and Systems Magazine 10 (2010) 40–50.

[8] Q. Chen, B. Li, W. Yin, X. Jiang, X. Chen, Bifurcation, chaos and fixed-time synchronization of memristor cellular neural networks, Chaos, Solitons & Fractals 171 (2023) 113440.

[9] C. Z. Aguilar, J. Gómez-Aguilar, V. Alvarado-Martínez, H. Romero-Ugalde, Fractional order neural networks for system identification, Chaos, Solitons & Fractals 130 (2020) 109444.

[10] M. I. Rabinovich, P. Varona, A. I. Selverston, H. D. Abarbanel, Dynamical principles in neuroscience, Reviews of Modern Physics 78 (2006) 1213–1265.

[11] D. Vignesh, S. He, S. Banerjee, A review on the complexities of brain activity: insights from nonlinear dynamics in neuroscience, Nonlinear Dynamics 113 (2025) 4531–4552.

[12] P. Selvaraj, O. Kwon, R. Sakthivel, Disturbance and uncertainty rejection performance for fractional-order complex dynamical networks, Neural Networks 112 (2019) 73–84.

[13] M. S. Ali, G. Narayanan, V. Shekher, H. Alsulami, T. Saeed, Dynamic stability analysis of stochastic fractional-order memristor fuzzy bam neural networks with delay and leakage terms, Applied Mathematics and Computation 369 (2020) 124896.

[14] M. S. Tavazoei, M. Haeri, A note on the stability of fractional order systems, Mathematics and Computers in Simulation 79 (2009) 1566–1576.
[15] C. Xu, M. Liao, P. Li, Y. Guo, Q. Xiao, S. Yuan, Influence of multiple time delays on bifurcation of fractional-order neural networks, Applied Mathematics and Computation 361 (2019) 565–582.
[16] M. Xiao, W. X. Zheng, G. Jiang, J. Cao, Undamped oscillations generated by hopf bifurcations in fractional-order recurrent neural networks with caputo derivative, IEEE Transactions on Neural Networks and Learning Systems 26 (2015) 3201–3214.
[17] S. Agrawal, M. Srivastava, S. Das, Synchronization of fractional order chaotic systems using active control method, Chaos, Solitons & Fractals 45 (2012) 737–752.
[18] M. S. Tavazoei, M. Haeri, Synchronization of chaotic fractional-order systems via active sliding mode controller, Physica A: Statistical Mechanics and its Applications 387 (2008) 57–70.
[19] K. L. Cooke, Z. Grossman, Discrete delay, distributed delay and stability switches, Journal of Mathematical Analysis and Applications 86 (1982) 592–627.
[20] C. Marcus, R. Westervelt, Stability of analog neural networks with delay, Physical Review A 39 (1989) 347.
[21] C. Huang, H. Liu, T. Huang, J. Cao, Bifurcations due to different neutral delays in a fractional-order neutral-type neural network, IEEE Transactions on Emerging Topics in Computational Intelligence 8 (2024) 563–575.
[22] P. Kumar, T. H. Lee, V. S. Erturk, A novel fractional-order neutral-type two-delayed neural network: Stability, bifurcation, and numerical solution, Mathematics and Computers in Simulation 232 (2025) 245–260.
[23] H. Wang, C. Huang, S. Liu, J. Cao, H. Liu, Bifurcation detection of a neutral-type fractional-order delayed neural network via stability switching curve, Nonlinear Dynamics 113 (2025) 3781–3790.
[24] Q. Song, Z. Zhao, Y. Liu, F. E. Alsaadi, Mean-square input-to-state stability for stochastic complex-valued neural networks with neutral delay, Neurocomputing 470 (2022) 269–277.
[25] Y. Wang, J. Cao, C. Huang, Bifurcations of a fractional three-layer neural network with different delays: Delay-dependent and order-dependent, Physica A: Statistical Mechanics and its Applications 633 (2024) 129431.
[26] C. Huang, H. Wang, H. Liu, J. Cao, Bifurcations of a delayed fractional-order bam neural network via new parameter perturbations, Neural Networks 168 (2023) 123–142.
[27] C. Huang, H. Wang, J. Cao, Fractional order-induced bifurcations in a delayed neural network with three neurons, Chaos: An Interdisciplinary Journal of Nonlinear Science 33 (2023) 033143.
[28] C.-A. Popa, Neutral-type and mixed delays in fractional-order neural networks: Asymptotic stability analysis, Fractal and Fractional 7 (2023) 36.
[29] C.-A. Popa, Asymptotic and mittag–leffler synchronization of fractional-order octonion-valued neural networks with neutral-type and mixed delays, Fractal and Fractional 7 (2023) 830.
[30] C. Huang, S. Mo, Z. Wu, Novel results on bifurcations for a fractional-order neural network with neutral delays, Fractals 30 (2022) 2250118.
[31] S. Li, X. Song, C. Huang, Investigation of delay-induced hopf bifurcation in a fractional neutral-type neural network, Fractal and Fractional 9 (2025) 189.
[32] B. N. Lundstrom, M. H. Higgs, W. J. Spain, A. L. Fairhall, Fractional differentiation by neocortical pyramidal neurons, Nature Neuroscience 11 (2008) 1335–1342.
[33] C. Xu, D. Mu, Z. Liu, Y. Pang, M. Liao, P. Li, L. Yao, Q. Qin, Comparative exploration on bifurcation behavior for integer-order and fractional-order delayed bam neural networks, Nonlinear Analysis: Modelling and Control 27 (2022) 1030–1053.
[34] J. Sieber, C. A. Alonso, A. Didier, M. N. Zeilinger, A. Orvieto, Understanding the differences in foundation models: Attention, state space models, and recurrent neural networks, Advances in Neural Information Processing Systems 34 (2024) 134534–134566.
[35] C. Huang, H. Liu, H. Wang, M. Xiao, J. Cao, Dynamical bifurcations of a fractional-order bam neural network: Nonidentical neutral delays, IEEE Transactions on Network Science and Engineering 11 (2023) 1668–1679.
[36] I. Podlubny, Fractional Differential Equations: An introduction to fractional derivatives, fractional differential equations, to methods of their solution and some of their applications, Academic Press, New York, 1999.

[37] W. Wang, Y. Qiao, J. Miao, L. Duan, Dynamic analysis of fractional-order recurrent neural network with caputo derivative, International Journal of Bifurcation and Chaos 27 (2017) 1750181.
[38] C. Huang, L. Fu, H. Wang, J. Cao, H. Liu, Extractions of bifurcation in fractional-order recurrent neural networks under neurons arbitrariness, Physica D: Nonlinear Phenomena 468 (2024) 134279.
[39] V. Claus, G. Deweß, M. Deweß, V. Diekert, B. Fuchssteiner, S. Gottwald, S. Gündel, J. Hoschek, E.-R. Olderog, M. Richter, et al., Teubner-Taschenbuch der Mathematik:Teil II, Wiesbaden: Academic Press, 2003.
[40] H. Wang, Y. Yu, G. Wen, Stability analysis of fractional-order hopfield neural networks with time delays, Neural Networks 55 (2014) 98–109.
[41] W. Deng, C. Li, J. Lü, Stability analysis of linear fractional differential system with multiple time delays, Nonlinear Dynamics 48 (2007) 409–416.
[42] K. Diethelm, N. J. Ford, A. D. Freed, A predictor-corrector approach for the numerical solution of fractional differential equations, Nonlinear Dynamics 29 (2002) 3–22.
[43] J. D. Kong, P. Salceanu, H. Wang, A stoichiometric organic matter decomposition model in a chemostat culture, Journal of Mathematical Biology 76 (2018) 609–644.